Suzan Miah, Md; Khan, Ahsan Noor; Icheln, Clemens; Haneda, Katsuyuki; Takizawa, Ken Ichi

Antenna system design for improved wireless capsule endoscope links at 433 MHz

Published in:
IEEE Transactions on Antennas and Propagation

DOI:
10.1109/TAP.2019.2900389

Published: 01/04/2019

Document Version
Peer-reviewed accepted author manuscript, also known as Final accepted manuscript or Post-print

Please cite the original version:
Suzan Miah, M., Khan, A. N., Icheln, C., Haneda, K., & Takizawa, K. I. (2019). Antenna system design for improved wireless capsule endoscope links at 433 MHz. *IEEE Transactions on Antennas and Propagation*, *67*(4), 2687-2699. Article 8648490. https://doi.org/10.1109/TAP.2019.2900389

Antenna System Design for Improved Wireless Capsule Endoscope Links at 433 MHz

Md. Suzan Miah, Ahsan Noor khan, Clemens Icheln, Katsuyuki Haneda, *Member, IEEE*, and Ken-ichi Takizawa

***Abstract*—Wireless capsule endoscopy (WCE) systems are used to capture images of the human digestive tract for medical applications. The antenna is one of the most important components in a WCE system. In this paper, we present novel small antenna solutions for a WCE system operating at the 433 MHz ISM band along with a link budget analysis. The in-body capsule transmitter uses an ultrawideband outer-wall conformal loop antenna, whereas the on-body receiver uses a printed monopole antenna with a partial ground plane. A colon-equivalent tissue phantom and CST Gustav voxel human body model were used for the numerical studies of the capsule antenna. The simulation results in the colon-tissue phantom were validated through *in-vitro* measurements using a liquid phantom. According to the phantom simulations, the capsule antenna has -10 dB impedance matching from 309 to 1104 MHz. The ultrawideband characteristic enables the capsule antenna to tolerate the detuning effects due to electronic modules in the capsule and due to the proximity of various different tissues in gastrointestinal tracts. The same design methodology was applied to on-body antennas followed by *in-vitro* and *ex-vivo* measurements for validation. The on-body antenna exceeds -10 dB impedance matching from 385 MHz to 502 MHz both in simulations and measurements. The path loss for the radio link between an in-body capsule transmitter and an on-body receiver using our antenna solutions, in simulations and measurements, is less than 50 dB for any capsule orientation and location, ensuring sufficient signal level at the receiver, hereby enabling an improved capsule endoscope.**

***Index Terms*—Conformal antenna, in-to-on body propagation, wireless capsule endoscope.**

I. INTRODUCTION

Wireless capsule endoscopy (WCE) is used to record images of the digestive tract for medical applications [1], [2]. In this technique, the patient swallows a small capsule with an embedded camera. The capsule moves through the gastrointestinal (GI) tract and captures images, which are transmitted to a receiver unit outside the body of the patient. A physician interprets these images either in real-time or offline.

The ability to transmit high-quality images at a high frame-rate is limited by the signal-to-noise ratio (SNR) of the radio link between the in-body capsule and the on-body or off-body receiver. An improved WCE needs antenna systems that realize lower path loss. The path loss inside human tissue is generally smaller at lower frequencies and it has been shown that in practice the optimal operating frequency for the radio link between in-body transmitter and external receiver is around 450 MHz [3], [4]. In [5] the path loss requirement for an improved WCE system, i.e. with a capacity of 2.0 Mbps enabling the transmission of 6 high-quality images per second, is derived through link budget analysis at 400 MHz. Transmit power was given in effective isotropic radiated power (EIRP) without considering realistic antennas. Another work in the framework of IEEE 802.15.6 standardization [6] demonstrated the link margin for a specific physical layer under a fixed path loss. Neither of these papers considers the effect of realistic in-body antennas on the path loss.

A. Review of Radio Link Studies

Many studies exist on the radio link of WCE systems, e.g., [7]–[10], [10]–[13], [13]–[18]. The in-body-to-on-body (IB2OB) link models discussed in [10], [13]–[15] consider frequencies above 1 GHz, leading to higher path loss compared to below 1 GHz. Additionally, papers [7]–[13], [18] present IB2OB radio links, where the outside-body antenna is not in contact with the body. Placing the receiving antenna close to the human abdomen instead of further away achieves a smaller path loss [19]. Radio links operating at 402 MHz, 868 MHz, and 2400 MHz are discussed in [16]. However, the paper considers unrealistically large antenna systems for practical WCE systems. In [17] a WCE operating at 433 MHz is presented without specific information about the on-body antenna. Finally, no paper reports robust antenna systems for WCE that work reliably at various positions and orientations of the antennas. It has been reported that in-body antenna positions and orientations impact the link path loss [20]–[23]. This paper provides a novel antenna system and a comprehensive analysis of link path loss based on the antenna system. Our antenna system shows very low path loss, enabling the improved WCE discussed in [5]. For practical reasons we choose the 433 MHz industrial, scientific and medical (ISM) system band for our design.

B. Review of In-body Capsule Antennas

The in-body antenna needs to be fitted into a small capsule, and the bandwidth requires to be wide enough to overcome the detuning effects due to varying tissue properties throughout the GI tract. Recent research has shown embedded [24]–[33] and conformal structures [7], [9], [17], [34]–[41], [43]–[45] as promising capsule antenna types. Embedded antennas

Manuscript received Month Day, Year; revised Month, Day, Year; accepted Month, Day, Year. Date of publication Month, Day, Year; date of current version Month, Day, Year.

M. S. Miah, K. Haneda and C. Icheln are with the Department of Electronics and Nanoengineering, Aalto University-School of Electrical Engineering, Espoo FI-00076, Finland. (e-mail: md.miah@aalto.fi).

A.N. Khan was with the Department of Electronics and Nanoengineering, Aalto University-School of Electrical Engineering, Espoo FI-00076, Finland. (e-mail: ahsannoorkhan@gmail.com).

K. Takizawa is with the National Institute of Information and Communications Technology (NICT), 3-4 Hikarino-oka, Yokosuka, Japan 2390847. (e-mail: takizawa@nict.go.jp).

TABLE I

A COMPARISON OF REPORTED CAPSULE ANTENNAS IN THE LITERATURE OPERATING UP TO 1000 MHz: ANTENNA TYPE, THE RESONANCE FREQUENCY, CAPSULE SIZE, IMPEDANCE MATCHING BANDWIDTH, RADIATION PERFORMANCE IN THE REPORTED PHANTOM ARE SUMMARIZED

Ref.	Antenna type	Freq. (MHz)	Capsule Size (mm)	Bandwidth (MHz)	Gain (dBi)	Phantom: tissue, shape, size (mm)
[24]	Embedded, loop	315		2		$\varepsilon_r = 58.0, \sigma = 0.77$ S/m, cube, 640^3
[25]	Embedded, multilayer PIFA	403	32 × 10	9	−29	Muscle, cyl., Ø80 × 110
[26]	Embedded, microstrip	915		11		Human body phantom
[27]	Embedded, helical	402		32		$\varepsilon_r = 56.0, \sigma = 0.8$ S/m, cyl., Ø75
[28]	Embedded, spiral	402	25 × 10.5	70		$\varepsilon_r = 56.0, \sigma = 0.83$ S/m, cyl., Ø150 × 150
[29]	Embedded, fat-arm spiral	450	25 × 10.5	75		$\varepsilon_r = 56.0, \sigma = 0.83$ S/m, cyl. Ø150 × 150
[30]	Embedded, dual-spiral	402		98		$\varepsilon_r = 56.0, \sigma = 0.83$ S/m, cyl., Ø150 × 150
[31]	Embedded, conical spiral	450		101		$\varepsilon_r = 56.0, \sigma = 0.83$ S/m, cyl., Ø150 × 150
[32]	Embedded, spiral	500		104	−19.9	$\varepsilon_r = 56.9, \sigma = 0.97$ S/m, cyl., Ø150× 150
[33]	Embedded, dual-spiral	402		189		$\varepsilon_r = 56.0, \sigma = 0.83$ S/m, cyl., Ø150
[7]	Conformal, inner-wall microstrip	434	17 × 7	17	−22	Muscle, sphere, Ø100
[34]	Conformal, outer-wall helix	433	30 × 10	20	−40.9	Muscle, cube, 190^3
[35]	Conformal, outer-wall microstrip	402	28 × 11	39.9	−29.6	Muscle, cube, 100^3
[36]	Conformal, microstrip	433	28.5 × 10	50	−9.6	$\varepsilon_r = 58.1, \sigma = 0.83$ S/m, cyl.
[9]	Conformal, microstrip	434	17 × 7	53	−33	$\varepsilon_r = 49.6, \sigma = 0.51$, cyl., Ø 200
[17]	Conformal, inner-wall patch	433	25 × 12	124.4	−36.9	$\varepsilon_r = 56.4, \sigma = 0.82$, cyl. Ø 100 × 200
[37]	Conformal, dipole	402	24 × 11	158	−37	Skin, cube, 180^3
[38]	Conformal, inner-wall loop	915	26 × 11	185	−19.4	$\varepsilon_r = 55.0, \sigma = 0.95$ S/m, cube, 100^3
[39]	Conformal, outer-wall loop	500	24 × 11	260		$\varepsilon_r = 56.4, \sigma = 0.82$, cyl. Ø150
[40]	Conformal, outer-wall PIFA	403	21 × 6	541	−31.5	$\varepsilon_r = 56.0, \sigma = 0.8$ S/m, Human body phantom
[41]	Conformal, outer-wall loop	500	21 × 11	785*		$\varepsilon_r = 56.4, \sigma = 0.82$, box, 200 × 150 × 100
[42]	Conformal, outer-wall loop	500	25 × 10	≈2200†		muscle, elliptic cylindrical, 180 × 100 × 50
This paper	Conformal, outer-wall loop	433	27 × 11	795	−35	$\varepsilon_r = 62.0, \sigma = 0.87$, box, 235 × 220 × 100

* Only simulation results have been reported.

† [42] proposes an implantable loop antenna for biomedical telemetric applications, but the matching behaviors under realistic operation environments of the capsule antenna were not studied.

are placed inside the capsule cavity. The conformal structure utilizes only the surface of the capsule module and leaves the interior for other components. It allows the most effective use of the available surface area of the capsule so that the antenna to be larger for better radiation performance [39]. In order for the capsule antennas to be insensitive to surrounding human tissue, magnetic antennas such as loop antennas are preferred over electric antennas [24], [46]. Table I shows a comparison of reported capsule antennas in the literature operating up to 1000 MHz. In [42] an implantable loop antenna is presented with −10 dB impedance matching from 300 MHz to about 2500 MHz. The implantable antenna was simulated in a human arm model composed of muscle tissue, so its applicability to WCE is not obvious. Among the reported capsule antennas for the WCE systems, [41] reports an outer-wall conformal antenna with the widest −10 dB impedance matching bandwidth, denoted as $\mathrm{BW}_{-10\mathrm{dB}}$ hereinafter, of 785 MHz. However, the paper did not report experimental validation of the matching. More importantly, none of the reported antenna solutions discusses implications on link path loss. In this paper, we propose a novel ultrawideband capsule antenna that realizes superior $\mathrm{BW}_{-10\mathrm{dB}}$ to existing designs and study its implications on link path loss.

C. Review of On-body Antennas for WCE

The on-body antenna should be compact and planar so that it can be easily attached to the abdomen of the patient. The antenna should also show wideband impedance matching to tolerate possible detuning effects during installation to different patients and body parts. In literature, we find several designs of on-body antennas [10], [13]–[15], [23], [47], but they focus on frequencies above 500 MHz. A summary of reported planar on-body antennas working below 500 MHz is shown in Table II. The antennas in [48]–[50] are not in direct contact to the skin. In [51] a monopole dual-band antenna with $\mathrm{BW}_{-10\mathrm{dB}} = 90$ MHz is presented. However, the antenna was evaluated with a human arm model, so its performance on the human abdomen is not obvious. Our design of on-body monopole antenna takes advantage of two existing methods, i.e., 1) modification of ground plane geometry and 2) addition of inductive patch, which have not been exploited together. The combination of two methods allows us to bring the resonant frequency to as low as 433 MHz while achieve the widest $BW_{-10\mathrm{dB}}$ in the literature, making our antenna most robust to detuning effects during installation and operation of the WCE. We realized the intended performance with the compact on-body antenna size as illustrated in Table II.

TABLE II

A SUMMARY OF REPORTED PLANAR ON-BODY ANTENNAS IN THE LITERATURE: THE RESONANCE FREQUENCY BANDS, ANTENNA DIMENSIONS, $\mathrm{BW}_{-10\mathrm{dB}}$

Ref.	Frequency bands [in MHz]	Dimensions [in mm]	$\mathrm{BW}_{-10\mathrm{dB}}$ [in MHz]
[48]	403	60 × 70	6
[49]	403	40 × 40	7
[51]	403	26.8 × 28	90
[50]	433	140 × 80	-*
This paper	433	59 × 52	117

* Matching level is higher than −10 dB at the lower band.

D. Summary of Novelty and Contributions

With the proposed in-body loop and the on-body antennas, this is the first paper that studies their implications on path loss, considering effects of capsule orientation and position, in order to demonstrate the suitability of the proposed antenna systems for improved WCE. The contributions of this paper are therefore threefold:

a) Demonstrating an IB2OB radio link with low enough path loss to maintain sufficient SNR at the on-body receiver for the improved WCE [5], regardless of in-body capsule locations and orientations; for this purpose, we develop
b) Novel ultrawideband conformal outer-wall loop antenna for capsule transmitter. The $\mathrm{BW}_{-10\mathrm{dB}}$ of the capsule antenna is 795 MHz, significantly outperforming the state-of-the-art [40] of 254 MHz; and,
c) Novel on-body receiver monopole antenna with a small size of 59 mm $\times$ 52 mm, while showing the resonance at 433 MHz and a very wide $\mathrm{BW}_{-10\mathrm{dB}}$ of 117 MHz.

The remainder of this paper is organized as follows. Section II illustrates the proposed capsule antenna configuration and simulations, while on-body antenna structure and simulations are described in Section III. Section IV addresses the experimental validation of the capsule and on-body antenna, and path loss. Finally, Section V concludes this paper.

II. Capsule Antenna Design and Simulations

A. Antenna Structure

The proposed antenna is a loop antenna patterned on a 100 μm thick flexible substrate Preperm 255, which allows bending and wrapping around the capsule. Relative permittivity, ε_r, and loss tangent, $\tan\delta$, of the substrate are 2.55 and 5.0×10^{-4}, respectively. Copper of 19 μm thickness is used as a conductor material on the substrate. The proposed antenna before and after wrapping it around the capsule is shown in Fig. 1. The antenna utilizes the outer-wall of the cylinder and one dome of the capsule module, whereas the other dome remains free for the camera and other optical components. The capsule module is made of polystyrene with $\varepsilon_\mathrm{r} = 2.6$ and $\tan\delta = 0.05$ at 1 GHz. The thickness of the capsules' wall, diameter, and length of the capsule are 0.5 mm, 11 mm and 27 mm, respectively. The antenna does not have a ground plane in order to avoid strong mirror current, which reduces antenna efficiency. Besides other parameters of the antenna change compared [52], an additional slot has been introduced in each loop arm as shown in Fig. 1(a) to enhance bandwidth. The dimensions of the loop have been optimized to resonate at 433 MHz as summarized in Table III. The feeding point of the antenna in the simulations is indicated by a red triangle in Fig. 1(b). The proposed capsule antenna is an extension of the authors' own work [52]. The technical advances of the present paper compared to [52] include i) improved bandwidth by optimizing antenna structure and dimensions, ii) numerically evaluating resonance and radiation performance using a single-layer colon phantom as well as a CST Gustav voxel human body model, iii) conforming the antenna on a realistic capsule module and iv) a study of the specific absorption rate (SAR).

B. Capsule Implementation and Operating Environments

A single-layer colon-tissue phantom model with dimensions of 235 mm $\times$ 225 mm $\times$ 100 mm was used for designing and optmizing the proposed antenna. The antenna arrangement in Fig. 1(b) was implanted at the center of a colon tissue phantom as visualized in Fig. 2. Since the colon is one of the

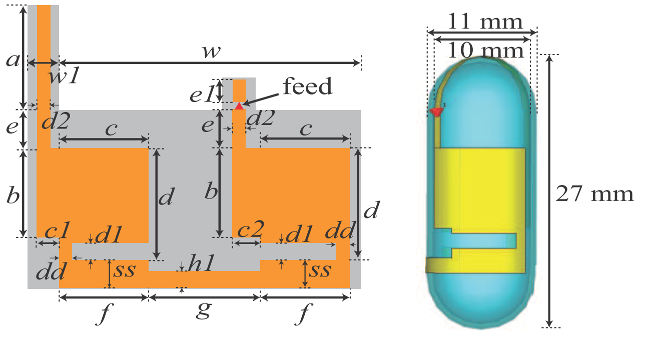

(a) (b)

Fig. 1. Capsule antenna (a) before, and (b) after placing around the capsule.

TABLE III
Optimized Dimensions of the Capsule Antenna Structure in mm

a	b	c	d	e	f	g	$c1$	$c2$	$d1$	$d2$	$e1$	dd	ss	$h1$	w	$w1$
14.7	8	8	10	3.5	8	10	2	2.5	1.5	1.2	2	1.5	2.5	1.5	31.4	3.2

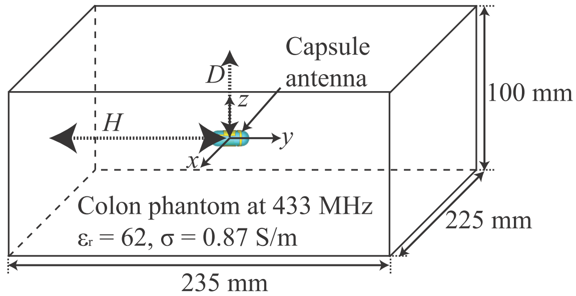

Fig. 2. The capsule endoscope antenna in the single tissue phantom model, where the dielectric properties of the colon-tissue have been used.

organs of the human GI tract, we used a colon-tissue phantom instead of widely used muscle tissue. The dielectric properties of the colon tissue are frequency dependent, and for 433 MHz they are listed in Table IV. We considered the frequency dependency when simulating antenna matching across a wider bandwidth centered at 433 MHz. The CST Studio Suite 2017 was used for the simulations.

1) A Reference Case: First, the capsule antenna without biocompatible layer and electronic components in the capsule was placed in the center of the colon-tissue phantom as shown in Fig. 2; Y-oriented means that the longest dimension of the capsule is aligned with the Y-axis. The distance between the center of the capsule to the top of the phantom, D and to the side wall of the phantom, H are 50 mm and 117.5 mm, respectively. Fig. 3 shows the simulated magnitude of a reflection coefficient, $|S_{11}|$. The antenna exhibits double resonances, at 438 MHz and 905 MHz. The -10 dB impedance matching is achieved across 309 MHz to 1104 MHz, which covers the entire band of interest. The peak realized gain of the antenna is -35 dBi at 433 MHz, whereas radiation efficiency is -37 dB (0.02%). Since antenna operates inside the very lossy medium, the low radiation efficiency is expected. The E-plane and H-plane cuts of the simulated realized gain patterns of antenna are shown in Fig. 4. It can be seen that the proposed antenna shows omnidirectional radiation pattern. Note that the peak realized gain of the antenna is affected by the distance from the body surface. In the following studies, this serves as

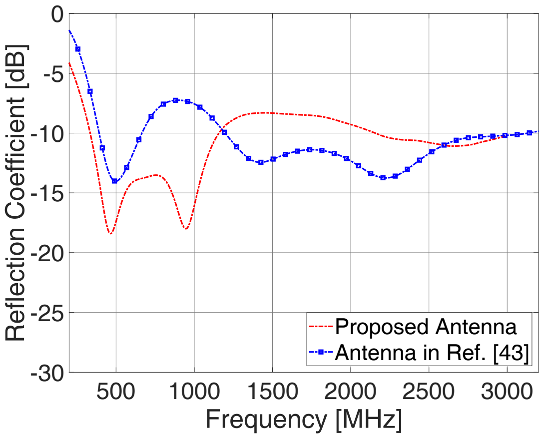

Fig. 3. Simulated reflection coefficient of the Y-orientated proposed and antenna in [42] at the center of the colon-tissue phantom.

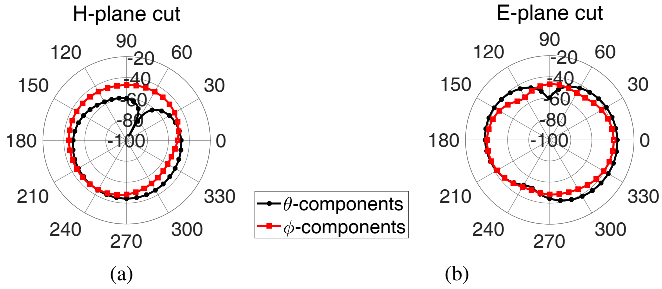

Fig. 4. Simulated farfield realized gain patterns of the Y-axis oriented capsule antenna at the center of the colon-tissue phantom in (a) H-plane cut, and (b) E-plane cut at 433 MHz (coordinate system defined in Fig. 2).

the baseline, and the above-mentioned settings and the same colon-tissue model are used unless otherwise stated.

2) Comparison with the Existing Design: An implantable loop antenna was presented in [42]. It was wrapped on the outer-wall of a cylinder made of propylene with the diameter of 10 and length of 15 mm. The compact size and ultrawideband impedance bandwidth make it a potential candidate for a capsule endoscope. However, the operating environment of the WCE was not considered when evaluating antenna performance. We recreated the antenna and wrapped on the outer-wall of a capsule with the dimensions of 25 mm × 10 mm including two domes. The thickness of the capsule wall and dielectric properties are the same as defined in Section II-A. A battery made of copper with the dimension of 7.5 mm × 6 mm as defined in [42] was placed in the center of the capsule, whereas remaining space was filled with air. The Y-oriented capsule was placed in the center of the colon-tissue phantom as shown in Fig. 2. The simulated $|S_{11}|$ is compared with our proposed antenna in Fig. 3. The existing design shows $\mathrm{BW}_{-10\mathrm{dB}}$ of 271 MHz centered at 500 MHz and at above 1 GHz. Our design shows much wider $\mathrm{BW}_{-10\mathrm{dB}}$ at the target band below 1 GHz and hence more robust against changes in the environment, e.g., different tissues in the GI tract. In addition, the simulated realized gain of the antenna in [42] at 433 MHz is -38 dBi, which is 3 dB smaller than the proposed antenna. Our capsule antenna outperforms the existing design in both bandwidth and realized gain at the target frequency band.

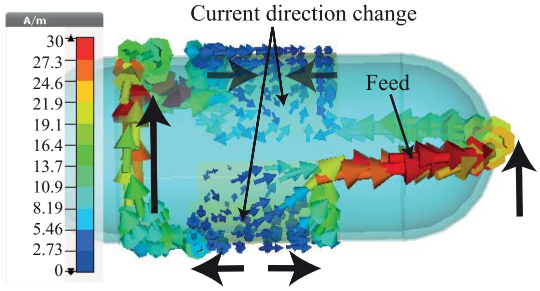

Fig. 5. Time snapshot of the current distribution of the capsule antenna at 433 MHz.

3) Operating Principle and Parametric Studies : To illustrate the antenna's operating principle, the current distribution of the antenna at the center of the phantom is presented in Fig. 5. With the optimized dimensions in Table III, the circumference of the loop is approximately one wavelength in the colon tissue at 433 MHz. Thus, the resonance of the antenna is caused by the mode of a typical full-wavelength loop. This means that on the loop we can observe two sections with oppositely phased currents, and two locations with zero current. The change of the current direction takes place at the center of the radiating loop arms. Due to the geometry chosen for the wrapped antenna, the maximum currents flow in the same direction at each end of the loop, as is illustrated in Fig. 5. This results in a constructive radiation by both current maxima.

For parametric studies, we consider the Y-oriented capsule antenna at the center of the phantom (see Fig. 2). The most important parameters of the proposed antenna design were the distance of the slot from the bottom of the antenna and the thickness of the slot dimension, i.e., ss and $d1$, respectively as indicated in Fig. 1(a). We begin investigating the effect of the slots on the antenna matching. Fig. 6(a) shows that the simulated $|S_{11}|$ with and without slots in the antenna geometry. The total physical length of the loop without slots is around 55 mm, which is approximately $\lambda_0/12$ where $\lambda_0 = 692$ mm is the wavelength of a radio wave at 433 MHz in vacuum. Since the loop is sandwiched between the substrate and lossy tissue, the effective relative permittivity for the combined substrate-tissue medium is approximately 32.3. With this effective permittivity, the 55 mm long loop inside the tissue medium is approximately a wavelength at 500 MHz, leading to a resonance shown in Fig. 6(a) with $\mathrm{BW}_{-10\mathrm{dB}}$ of 572 MHz. After introducing the slots with $ss = 5$ mm and $d1 = 1.5$ mm, another resonance appears at around 900 MHz. Thus, the bandwidth increased by 166 MHz by introducing the slots. Since the slots with $ss = 5$ mm do not increase the loop length, the first resonance remains at around 500 MHz.

Parametric studies have been performed to determine the position of the slots to shift the first resonance down to 433 MHz and to enhance the bandwidth. We changed ss from 5 mm to 1.5 mm. Fig. 6(b) shows the effect of the slot position on the resonance and bandwidth. With $ss = 1.5$ mm, the maximum physical loop length of 70 mm is achieved, thus the fundamental resonance shifted to 438 MHz, whereas second one remains at 905 MHz. Results show 57 MHz improvements in $\mathrm{BW}_{-10\mathrm{dB}}$ as we decrease ss from 5 to 1.5 mm. In addition,

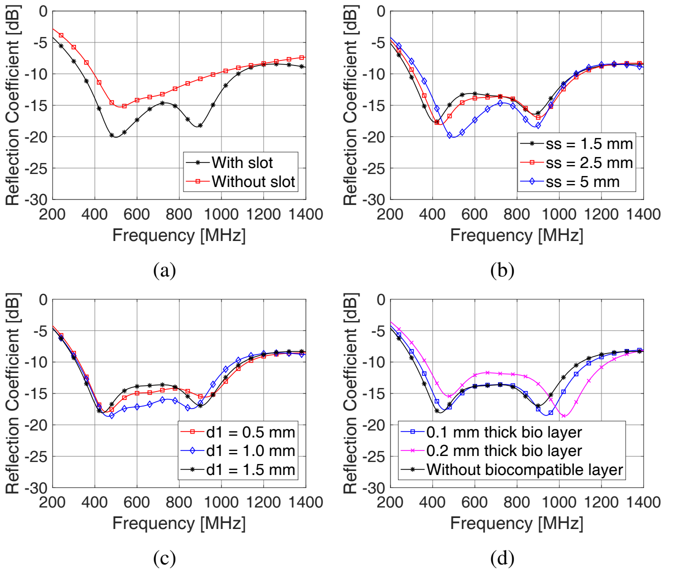

Fig. 6. Parametric studies the Y-orientated capsule antenna at the center of the colon-tissue phantom: (a) presence of the slots, (b) slots positions, (c) thickness of the slots, and (d) thcikness of the biocompatible layer.

TABLE IV
THE DIELECTRIC AND CONDUCTIVE PROPERTIES OF STOMACH, COLON AND SMALL INTESTINE AT 433 MHz [54]

Tissues	ε_r	σ [S/m]	$\tan\delta$
Stomach	67.2	1.01	0.62
Colon	62.0	0.87	0.58
Small Intestine	65.2	1.92	1.22
Muscle	56.9	0.8	0.59

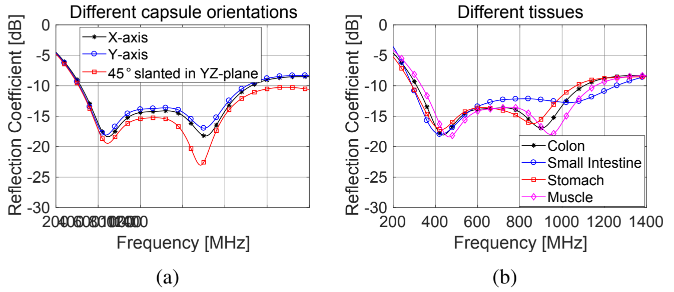

Fig. 7. Detuning effects of capsule antenna matching at the center of the colon-tissue phantom as in Fig. 2 due to (a) capsule orientations, and (b) different surrounding tissues.

Fig. 6(c) shows the effect of $d1$ on matching. The first resonance moves from 460 to 438 MHz as $d1$ increases from 0.5 to 1.5 mm. We found that the slots introduce an additional resonance for enhanced bandwidth, and that their dimensions and position determine the resonant frequency. For our goal to achieve a resonance at 433 MHz with maximum bandwidth, we choose ss and $d1$ to be 2.5 and 1.5 mm, respectively.

Biocompatibility is the property of materials that do not cause any toxic reactions, effects, or injuries in the human body. The materials also isolate the capsule from the moist and corrosive environment inside the GI tract. Because the antennas are made of non-biocompatible materials and they are on the outer-wall of the capsule, an introduction of a biocompatible insulation on the antenna is inevitable in practice. Required thickness of the biocompatible layer is studied for a popular material of low-loss Polyamide with $\varepsilon_r = 4.3$ and $\tan\delta = 0.004$ [53]. A Y-oriented capsule antenna with 0.1 mm and 0.2 mm thick Polyamide layer was simulated at the center of the colon-tissue phantom shown in Fig. 2. Fig. 6(d) shows the $|S_{11}|$ of the capsule antenna with and without biocompatible layer. As expected the antenna resonance shifts slightly up in frequency, because the biocompatible layer reduces the dielectric loading effect. However, $|S_{11}|$ remains below -10 dB between 400 and 600 MHz and maintains ultrawideband characteristic.

4) Effects of Capsule Orientations: As it is impossible to control the orientation of the capsule during endoscope operation, its orientation is considered random. We numerically evaluate the changes of antenna matching for three different orientations of the capsule at the center of the colon-tissue phantom in Fig. 2. Antenna matching for X-, Y- and 45° slanted in YZ-oriented capsule is shown in Fig. 7(a). The results demonstrate that the capsule orientation does not have a significant impact on the antenna resonance, as can be expected inside a large homogeneous phantom. The peak realized gain at 433 MHz of the X-oriented, Y-oriented and 45° slanted (in YZ-plane) capsule antenna is -34.5, -35 and -32 dBi, respectively. The variation of the peak gain across different orientation is not significant.

5) Effects of Different Tissues: As a capsule travels through the entire GI tract, it experiences a significant change of relative permittivity and conductivity depending on the surrounding tissues, as presented in Table IV [54]. Fig. 7(b) shows $|S_{11}|$ for different surrounding tissues of the phantom in Fig. 2, indicating slight decrease of the antenna's resonance frequency in the stomach and small intestine due to the higher ε_r than the colon. Furthermore, matching bandwidth is enhanced when the antenna is in the small intestine. Since the quality factor of the capsule antenna in the small intestine is the smallest due to the highest $\tan\delta$, the antenna shows the largest matching bandwidth among other tissues. As a muscle tissue phantom is frequently used for the performance evaluation of capsule antennas in literature [7], [25], [34], [35], [44], [55], we evaluated the antenna matching in muscle tissue as well. The antenna in muscle tissue resonates at a slightly higher frequency due to lower ε_r. Despite clear variations in the antenna resonance across tissue types, $|S_{11}|$ remains below -10 dB between 336 and 1065 MHz in all cases.

6) Effects of Electronic Components in the Capsule: The capsule transmitter comprises of electronic components, such as illuminating light, telemetry unit, camera, and battery, among which the battery occupies the largest volume. The effect of these electrical components on $|S_{11}|$ was numerically simulated for varying sizes of the battery and its position inside the capsule. The battery was modeled as a cylinder made of a perfect electric conductor with 7.5 or 8.5 mm diameters and 7.2 mm height and was placed at either the bottom or center of the capsule. Results are shown in Fig. 8 indicating that the battery with 8.5 mm diameter slightly increases the resonance frequency of the antenna compared to a hollow capsule. The antenna still maintained $|S_{11}|$ lower than -10 dB and a wide-enough matching bandwidth around 433 MHz.

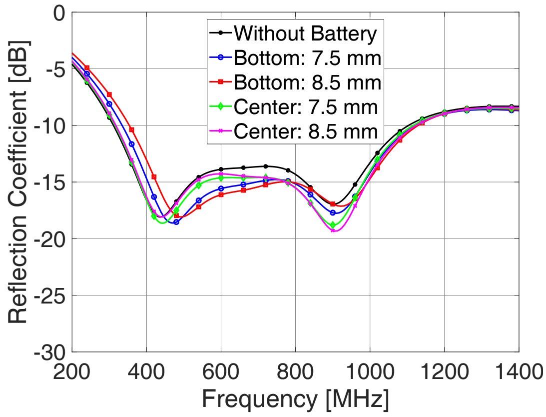

Fig. 8. Detuning effects of capsule antenna matching at the center of the colon-tissue phantom as in Fig. 2 due to batteries in various positions inside the capsule.

C. Resonance, Radiation, Specific Absorption Rate (SAR) in a Realistic Human Body Model

The resonance and radiation performance of the capsule antenna was studied with 3-D CST Gustav voxel human body model. The height and age of the male human model are 1760 mm and 38 years, respectively. Due to the limited computing resources, only a torso with the dimensions of $290 \times 230 \times 100\ \mathrm{mm}^3$ was considered, which is comparable with the dimensions of the single-layer colon phantom shown in Fig. 2. The origin of the coordinate system as well as three implant positions of the Y-oriented antenna in the human body model are illustrated in Fig. 9. When implanted in the colon, stomach, and small intestine, the capsule is approximately 50, 60 and 75 mm away from the nearest body surface, respectively. The simulated $|S_{11}|$ of the optimized capsule antenna without electronics and biocompatible layer with three implant positions are presented in Fig. 10. The results demonstrate that for the proposed antenna $|S_{11}|$ is better than -10 dB at 433 MHz for all implant positions and maintains a wide impedance matching bandwidth. A comparison of the results in Fig. 10 with those in Fig. 7(b) indicates the suitability of using the simplified colon phantom in Fig. 2 for the capsule antenna design. The simulated peak realized gain for the implant location in colon was -23.5 dBi, while it was -26 dBi for the antenna implanted at the same depth in the single-layer colon phantom shown in Fig. 2. The simulated peak realized gain is -26.8, and -29.7 dBi for the capsule antenna implanted in the stomach, and small intestine of the anatomical body phantom, respectively. The antenna in small intestine shows a lower peak gain due to the higher tissue conductivity compared to colon and stomach.

Since the capsule antenna needs to operate inside the human body, radiation safety should be discussed. There is a maximum allowable power radiated from the capsule antenna. The SAR is the rate of energy deposited per unit mass of tissue. The IEEE C95.1-1999 [56] and C95.1-2005 [57] specify that 1-g and 10-g averaged SAR should be less than 1.6 W/kg and 2 W/kg, respectively. The SAR calculator in CST Microwave Studio therefore numerically estimated the maximum allowable input powers to the Y-orientated capsule antenna implanted at three different positions in the CST Gustav voxel human body model. The results demonstrate that the capsule antenna is safe to be used at the transmit power less than 7.1 and 28 mW in colon, 5.0 and 24 mW in small intestine and 7.2 and 25 mW in stomach for the 1-g and 10-g averaged SAR, respectively. The low gain of -35 dBi of the capsule antenna along with the low transmit power of -10 dBm ensures that the EIRP is well below the regulated maximum $\mathrm{EIRP}_{\max}$ of -13 dBm at 433 MHz [58]. The next section deals with the on-body antenna designs and numerical studies.

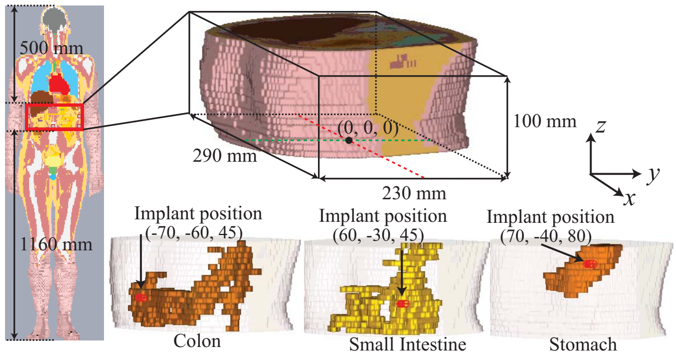

Fig. 9. 3-D Gustav Voxel human body model and three implant positions of the capsule.

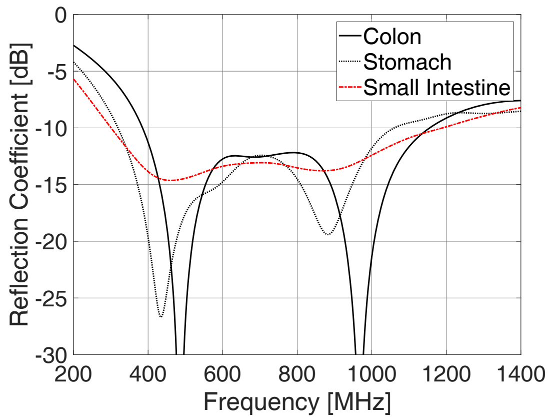

Fig. 10. Simulated reflection coefficient of the capsule antenna in CST Gustav voxel human body with three different positions, i.e., in colon, stomach and small intestine.

III. On-Body Antenna Designs and Simulations

Antennas of the receiver unit of a WCE system are placed directly on the human body. In the following subsections, we introduce our antenna, and optimize its dimension by studying resonance and radiation performance using the single-layer colon tissue phantom introduced in Section II-B. Furthermore, we evaluate them also using the 3-D CST Gustav voxel human body used in Section II-C. The simulation results of the antenna on a single-layer phantom will be compared to corresponding phantom measurements in Section IV-B, while results with the antenna on anatomical human body model will be validated through *ex-vivo* measurements on a test person.

A. Antenna Structure and Optimization

Printed monopole antennas have been considered as a suitable candidate for the on-body receiver unit of WCE systems

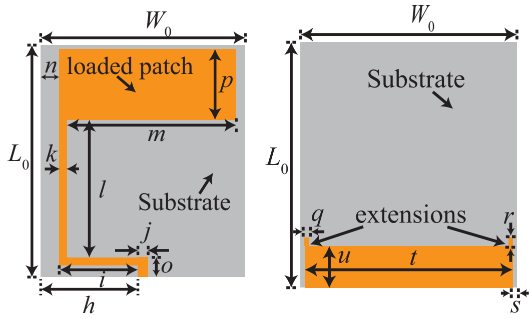

(a) (b)

Fig. 11. On-body antenna structure: (a) top view, and (b) bottom view.

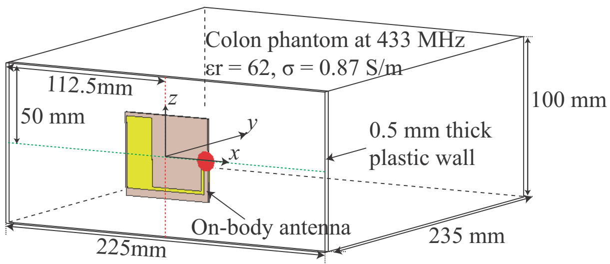

Fig. 12. Receiver antenna on a single-layer colon tissue phantom.

due to its planar shape, wideband matching, and easy miniaturization and manufacturing. A meandered arm monopole with a partial ground plane was used to realize a compact size and increase efficiency [59], improve impedance matching level and bandwidth [60], [61]. The proposed radiating meandered monopole was patterned on one side of the substrate and a partial ground plane was printed on the other side as illustrated in Fig. 11(a) and Fig. 11(b), respectively. A 1.5 mm thick FR4 with $\varepsilon_r = 4.3$ is used as the substrate, whereas 19 μm thick copper is used as a conductor to pattern the monopole and ground plane. A loaded patch at the end of the meandered monopole was added (see Fig. 11(a)) as a tuning structure. In addition, two small parallel extensions to the ground plane (see Fig. 11(b)) were added to increase its electrical length and they keep the resonance at 433 MHz.

The antenna was placed in the center of the outer wall of the colon-tissue phantom model as shown in Fig. 12. For consistency with set-ups of the measurement described in Section IV-A2, a 0.5 mm thick plastic container with $\varepsilon_r = 1.88$ and $\tan\delta = 0.005$ was included in the simulation model. An SMA edge connector was used as the antenna feed, but it prevented the antenna from being fully touching the surface of the phantom during measurement. So, this gap of 1 mm between the antenna and plastic container was introduced also in the simulations. Keeping all parameters constant and without any modifications to the ground plane, a parametric study was performed on the length of the loaded patch, i.e., p between 2 and 20 mm, which acts as an inductive loading element. With $p = 2$ mm, the antenna resonated at around 520 MHz with $\text{BW}_{-10\text{dB}}$ of 110 MHz and the resonance frequency decreased with increasing p. The maximum obtainable $\text{BW}_{-10\text{dB}}$ of 117 MHz was achieved for $p = 18$ mm, but the resonance frequency was slightly higher than desired. After adding two parallel extensions to the ground plane (see Fig. 11(b)) the

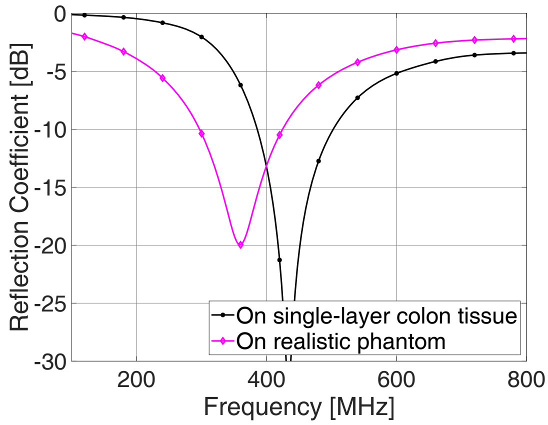

Fig. 13. Simulated reflection coefficient of the on-body antenna.

TABLE V
OPTIMIZED DIMENSIONS OF THE ON-BODY ANTENNA ON A SINGLE-TISSUE PHANTOM IN MM

L_o	W_0	h	i	j	k	l	m	n	o	p	q	r	s	t	u
59	52	24.7	20	2.6	2	35	43	4.7	5	18	1	2	1	49	10

resonance frequency was tuned to the desired 433 MHz as shown in Fig. 13, while $\text{BW}_{-10\text{dB}}$ remained 117 MHz. The optimized dimensions of the antenna are presented in Table V. The simulated peak realized gain is -18 dBi.

B. Antenna Performance on Realistic Human Body Model

The resonance and radiation performance of the antenna was evaluated using a 3-D CST Gustav voxel human body model. The dimensions of the human body torso used in the numerical simulations are same as in Section II-C. According to [22], the antenna was placed directly on the left-side abdominal skin of the torso. The simulated $|S_{11}|$ shown in Fig. 13 depicts that the antenna resonates at 360 MHz. The downward shift of the resonance frequency is reasonable since the antenna was in direct contact with the skin tissue. However, the antenna maintains the $|S_{11}|$ less then -10 dB at 433 MHz. The simulation results show the proposed antenna is indeed robust against different installations on the human body. The simulated peak realized gain of the antenna is -16.5 dBi. Finally, the SAR was estimated using CST Microwave Studio. We found that the maximum allowable input powers to the antenna placed on the abdomen of CST Gustav human body model are 18 and 82 mW for the 1-g and 10-g averaged SAR, respectively.

IV. ANTENNA FABRICATION AND MEASUREMENTS

A. Capsule Antenna

1) Fabrication: The fabricated capsule antenna before wrapping on the capsule module is presented in Fig. 14(a). Since a broadband surface mount balun and an SMA connector will be used to feed the antenna in the *in-vitro* measurement, the footprints of the balun and the SMA connector were also fabricated along with the antenna. The antenna was fabricated on the same flexible substrate material as defined in Section II-A; details of the fabrication process are described in [52]. The dimensions of the flat capsule antenna follow in Table III, and it was wrapped around the outer-wall of

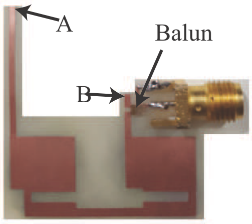

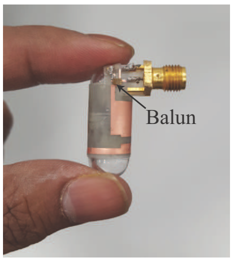

Fig. 14. Fabricated capsule antenna (a) before, and (b) after placed around the capsule.

a standard capsule module as illustrated in Fig. 14(b). The capsule module is made of polystyrene with $\varepsilon_{\mathrm{r}} = 2.6$ and $\tan\delta = 0.05$ at 1 GHz. The diameter and length of the capsule are 11 mm and 27 mm, respectively, whereas the thickness of the wall is 0.5 mm. After wrapping the points A and B in Fig. 14(a) were soldered together to form the loop. The biocompatible layer and any components inside the capsule were not included in the measurement.

2) Measurement Set-up: The *in-vitro* measurement set-up for the capsule antenna is illustrated in Fig. 15, which consisted of a vector network analyzer (VNA) and a rectangular-shaped plastic container forming the phantom. The container has approximately the same size as the phantom used in the simulations in Section II-B (see Fig. 2). It was filled with a liquid mimicking the colon tissue. The liquid was formulated by mixing 79% salted water and 21% TritonX-100. The mixing process consists of the following steps: dissolving the salt in distilled water as 7.85 g/L, and heating the TritonX-100 and salted water at $40°$C separately before mixing. We used HP 8720C network analyzer and 85070A dielectric probe kit [52] based on the transmission line propagation method to measure the electrical properties of the liquid phantom. The measured permittivity and loss tangent values at 433 MHz were 61.4 and 0.60, respectively, emulating the dielectric properties of the colon tissue properly.

Since the proposed loop antenna is balanced, the current leakage would be a possible problem when connecting with an unbalanced transmission line, such as, a coaxial cable. We used balun instead of the setup in [52] to measure the balanced capsule antenna using an unbalanced connector. For differential feeding, we used similar approach reported in [39]. A wideband surface mount balun (Analen B0322J5050AHF) was used at the feeding point of the antenna. Balance ports of the balun were connected to the antenna, whereas center and outer conductors of an SMA connector were soldered to the unbalanced port and ground of the balun, respectively. During the measurements, we used a layer of sticky rubber with $\varepsilon_{\mathrm{r}} = 2.2, \tan\delta = 5.0 \times 10^{-4}$ around the feeding components, i.e., a balun, an SMA connector, and a coaxial cable to avoid the direct contact with the liquid [25], [53]. As the VNA was calibrated on the reference plane of the SMA connector, capsule antenna with the SMA connector was simulated to test its impact on matching. Since the SMA connector was isolated from the liquid, we found a negligible impact on matching. The SMA connector inside the sticky rubber works

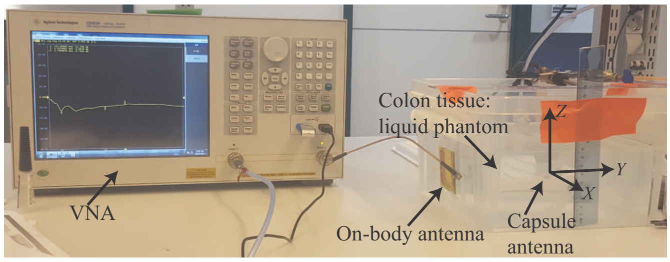

Fig. 15. Illustration of the matching and path loss measurement setups.

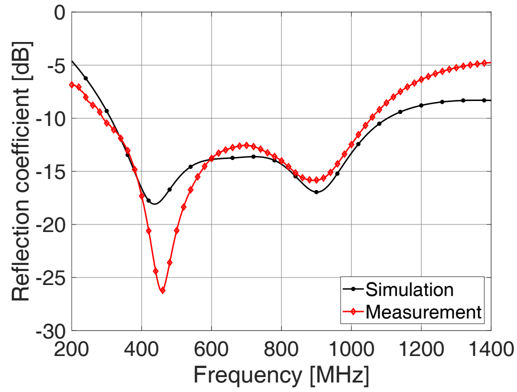

Fig. 16. Comparison of simulated and measured reflection coefficient: (a) Y-oriented capsule antenna at the center of the phantom; the simulated curve is identical to the one in Fig. 3.

almost as in free space at the designed frequency band. The proposed capsule antenna, which was inserted in the colon liquid phantom, was connected to port-1 of the VNA, while the port-2 in Fig. 15 was open-ended in matching measurements.

3) Results: The comparison of the simulated and measured $|S_{11}|$ of a Y-oriented capsule antenna at the center of the liquid phantom is presented in Fig. 16. The simulated plot is identical to the one in Fig. 3. The results show that the measured plot matches simulated one quite well. The lower resonance is slightly shifted upwards to 455 MHz, while the second resonance is at 905 MHz as in the simulations. The measured matching at 433 MHz is 5 dB better than in the simulations. This might come from the fabrication process of the prototype. Since the fabricated antenna was attached on the outer-wall of the capsule, there might be small air gaps between the antenna and capsule wall. The measured $|S_{11}|$ of the proposed capsule antenna is better than -10 dB across the frequency range from 280 MHz to 1057 MHz, which agrees well with the simulated matching bandwidth.

Several more measurements were performed with the different orientations of the capsule in the phantom as discussed in Section II-B4. Fig. 17 presents the comparison of simulated and measured $|S_{11}|$ of the antenna for three orientations of the capsule at the center of the phantom. Though slight differences in the resonance behavior are evident, the results show the robustness of the antenna design and experimentally validate the simulated results. The measured $|S_{11}|$ is better than -10 dB for at the target frequency band regardless of the capsule orientations. Table I shows a comparison of reported capsule antennas in the literature, designed frequencies are up to 1400 MHz. The matching bandwidth of the proposed

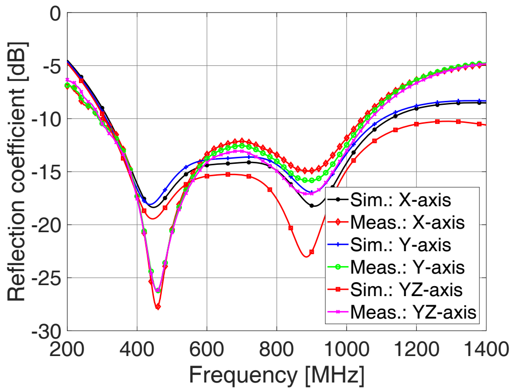

Fig. 17. Comparison of simulated and measured reflection coefficient for different orientations of the capsule at the center of the phantom; the simulation results are taken from Fig. 7(a).

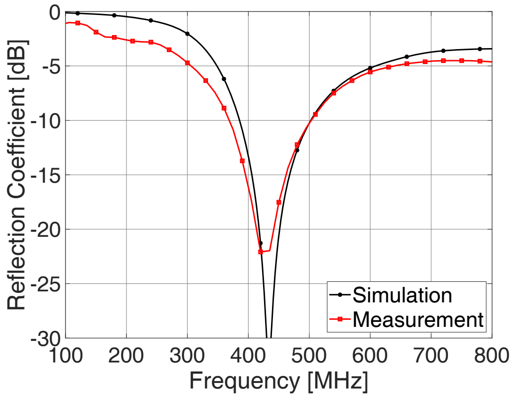

Fig. 18. Simulated and measured reflection coefficient of the on-body antenna on the liquid phantom; the simulation curve is taken from Fig. 13.

capsule antenna exceeds the existing solutions, while the realized peak gain is comparable. It should be noted that for amore accurate comparison of the realized gain, all solutions would need to be investigated in the same set-up using a phantom with identical geometry and dielectric properties.

B. On-Body Antenna

The on-body antenna was fabricated on the same FR4 substrate as in the simulation, detailed in Section III-A. The fabricated on-body monopole antenna is shown in Fig. 19(a). The *in-vitro* measurement was performed using the liquid phantom, introduced in Section IV-A2, and shown in Fig. 15. The on-body antenna was placed on the outer wall of the liquid container and connected to the VNA port-2 through a coaxial cable, while VNA port-1 was open-ended during this measurement. A good aggrement between the simulated and measured $|S_{11}|$ is achieved, as can be seen in Fig. 18. The antenna resonates at 420 MHz, with -10 dB impedance bandwidth of 120 MHz.

In addition to measurements with the phantom, the antenna matching was studied with a real human body of BMI 22 in a laboratory environment. In agreement with the simulations in Section III-B that use the realistic human body model, the *ex-vivo* measurements include the on-body antenna placed on the abdominal skin directly. Fig. 19(a) shows the *ex-vivo* measurement set-up. Fig. 19(b) presents the measured and simulated $|S_{11}|$ having a similar profile, though their

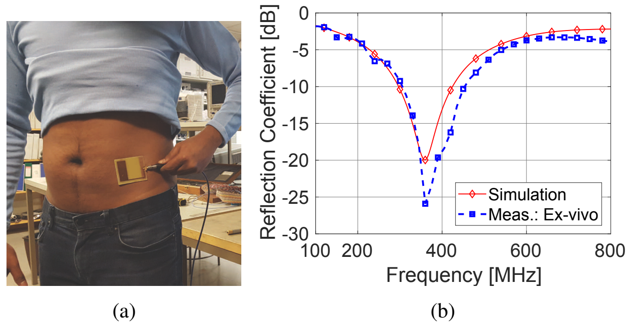

Fig. 19. (a) *Ex-vivo* measurement set-up of the on-body antenna, and (b) Simulated and measured reflection coefficient of the antenna, where the simulation results are taken from Fig. 13.

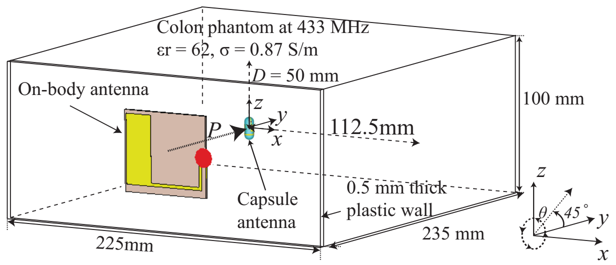

Fig. 20. Set-up for path loss simulation of the in-body to on-body radio link.

best matching level differs. Nevertheless, the on-body antenna resonates at 360 MHz as in the simulations with the CST Gustav voxel human body model. The comparison consistently shows better matching than -10 dB at 433 MHz.

C. Path Loss

The IB2OB link path loss was studied using the proposed antennas. The homogeneous colon tissue phantom model was considered both in simulations and measurements. The simulation uses a time domain full-wave solver. The path loss for a particular capsule and on-body antenna location is defined as the ratio of the input power at the transmit capsule antenna port to the output power at the on-body antenna port. In terms of transmission coefficient of the two-port network, it is expressed as $PL|_{\mathrm{dB}} = -10\log_{10}|S_{21}|$.

Fig. 20 illustrates the path loss simulation setup. Three different orientations of the capsule are considered, such that they are along the X-axis, Y-axis, and 45° slanted on the YZ-plane. For each orientation, the transmit-receive distance was changed by moving the capsule antenna along Y-axis away from the receive antenna, i.e., P increases, while maintaining the same $D = 50$ mm. The distance between the antennas includes 0.5 mm thickness of phantom's plastic container and 1 mm air gap between the on-body antenna and phantom's wall. The path loss was estimated at six distances between $P = 20$ to 120 mm for each of the above-mentioned capsule orientations. The corresponding *in-vitro* measurements were performed using the liquid phantom introduced in Section IV-A2 as shown in Fig. 15. The capsule and on-body antennas were connected to the VNA ports 1 and 2, respectively. The simulated and measured path loss are plotted together in Fig. 21, showing their close agreement for all the tested capsule orientations. The mean simulation path loss error is -0.4, -0.4 and -0.3 dB for the X-,

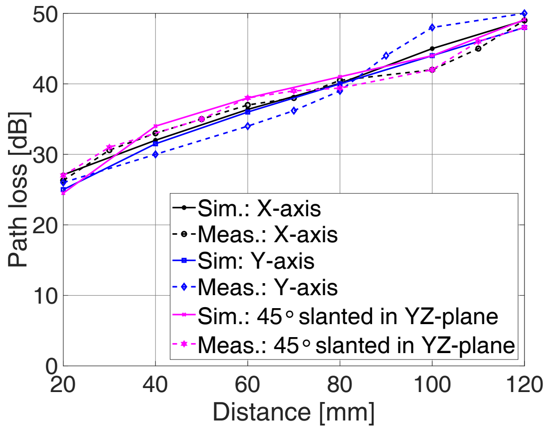

Fig. 21. The simulated and measured link path loss between in-body capsule and on-body antennas.

Y- and *YZ*-oriented capsule, respectively, whereas standard deviation is 1.3, 2.1 and 1.4 dB. The minimum path loss is observed when the capsule antenna is 45° slanted in the *YZ*-plane. The maximum path loss of 50 dB is observed in the measurement when capsule antenna is Y-oriented at the center of the phantom. The path loss differences across capsule orientations are mainly due to polarization mismatch between in- and on-body antennas. The simulated axial-ratio of fields towards $-Y$-axis direction at 433 MHz for the *YZ*-, *X*- and *Y*-oriented capsules at the center of the colon-tissue phantom is 8.4, 9 and 13 dB, respectively. The values indicate elliptical to linear polarization of the transmitted far-fields. The path loss of the Y-oriented capsule is slightly higher probably due to more pronounced polarization mismatch than in other orientations.

The robustness of the radio link across orientations was further checked through simulations. With the 120 mm separation between the antennas and $D = 50$ mm, the capsule was rotated on the YZ-plane with $\theta = 10°$ steps, as defined in Fig. 20. The maximum and minimum path loss were 49.3 and 46.6 dB at the θ angles of 60° and 290°, respectively; the 2.7 dB difference between maximum and minimum path loss may be attributed to the extent of polarization mismatch. The outage path loss for 5% probability is 49.2 dB. Regardless of antenna locations and orientations, the simulated and measured path loss was less than 50 dB.

D. System Requirements and Link budget

Finally, we show the link budget analysis to demonstrate that our antenna system enables the improved WCE presented in [5]. We adopted the same approach as reported in [5], but using the proposed realistic capsule and on-body antennas. Let us consider the images from the GI tract are compressed through loss-less JPEG coding technique, which has a compression rate of 0.5. The total number of pixels per image is 288×288 and each of those is compressed by 8-bit quantization levels. For this compression, the required data bit rate is 1.99 Mbps for a transmission of 6 images per second [5]. We considered uncoded Gaussian minimum shift keying (GMSK) as a modulation scheme, which is capable of providing the required bit rate and has been adopted as a mandatory for 420 to 450 MHz bands in IEEE 802.15.6 standard [6]. The receive SNR of 14 dB is required to maintain bit error rate (BER) less than 1×10^{-6} [62]. The input power to the capsule antenna port is set to -10 dBm. By considering the maximum measured path loss of 50 dB with our antenna system, the smallest received power at the on-body antenna is -60 dBm. Note that the measured path loss includes the gain of the antennas. The channel spans from 433.05 to 434.79 MHz and hence the bandwidth BW is 1.74 MHz. With 10 dB noise figure N_{F} at the receiver, the total noise power $N = -101.3$ dBm. Even after subtracting the fading margin $M = 10$ dB and implementation loss $IL = 6$ dB, we have the SNR of 25.3 dB, which is 11.3 dB larger than the required SNR to achieve BER less than 1×10^{-6}. Setting the link margin to be 0 dB the maximum acceptable path loss of 75.3 dB yields. The maximum measured path loss of 50 dB with our antenna system is 25.3 dB smaller than the maximum acceptable path loss. A summary of the link budget analysis is presented in Table VI. The proposed antenna solutions, therefore, are capable of supporting the improved WCE regardless of locations and orientations of the capsule.

TABLE VI
PARAMETERS OF THE LINK BUDGET FOR IMPROVED WCE SYSTEMS

Parameters	Values
Input power to the capsule antenna port, P_{t}	-10 dBm
Maximum measured path loss, PL	50 dB
Received power at on-body antenna port, $P_{\mathrm{r}} = P_{\mathrm{t}} - PL$	-60 dBm
Channel bandwidth, BW	1.74 MHz
Noise figure, N_{F}	10 dB
Temperature, T	310 K
Boltzmann constant, k	1.38×10^{-23}
Fading margin, M	10 dB
Installation loss, IL	6 dB
Noise level, $N = kTBW \cdot N_{\mathrm{F}}$	-101.3 dBm
Receive SNR after subtracting the fading margin, $\Gamma = P_{\mathrm{r}} - N - M - IL$	25.3 dB

V. CONCLUSION

In this paper, we present novel small antenna solutions of an improved WCE operating at 433 MHz ISM band. An ultrawideband conformal loop antenna is proposed for the in-body transmitting capsule, while the on-body receiving antenna is a printed monopole with a partial ground plane. The in-body antenna utilizes the outer-wall of the capsule and leaves the inner space for the other electronic components. For a required impedance matching of -10 dB, the proposed antenna supports a bandwidth of 795 MHz, from 309 to 1104 MHz. The ultrawideband matching enables the capsule antenna to overcome the detuning effects especially due to the proximity of the capsule to various different tissues in the GI tract. The on-body antenna was numerically evaluated on a colon-tissue phantom and on a realistic human body model. *In-vitro* measurements on a liquid phantom and *ex-vivo* measurements on a real human body were performed for validations. The measured -10 dB impedance matching from 384 MHz to 501 MHz shows good agreement with simulated results. The path loss for the radio link between an in-body capsule transmitter and an on-body receiver was studied using the proposed antenna solutions. The maximum link path loss penalty due to polarization mismatch was only

2.7 dB. Finally, the link budget analysis shows that the proposed antenna system is capable of maintaining high SNR at the receiver for all the capsule orientations and locations in the body, opening the way for improved ingestible WCE by supporting higher-data-rate radio links. Our future work includes implementation of dual-polarized antenna systems for WCE that utilizes polarization diversity.

REFERENCES

[1] G. Iddan, G. Meron, A. Glukhovsky, and P. Swain, “Wireless capsule endoscopy,” *Nature*, vol. 405, no. 6785, p. 417, May 2000.

[2] A. Kiourti, K. A. Psathas, and K. S. Nikita, “Implantable and ingestible medical devices with wireless telemetry functionalities: A review of current status and challenges,” *Bioelectromagnetics*, vol. 35, no. 1, pp. 1–15, 2014.

[3] A. Khaleghi, M. S. E. Sendi, R. Chavez-Santiago, F. Mesiti, and I. Balasingham, “Exposure of the human brain to an electromagnetic plane wave in the 100-1000 MHz frequency range for potential treatment of neurodegenerative diseases,” *IET Micro., Ant. Propag.*, vol. 6, no. 14, pp. 1565–1572, Nov. 2012.

[4] M. R. Basar, F. Malek, K. M. Juni, M. I. M. Saleh, M. S. Idris, L. Mohamed, N. Saudin, N. A. M. Affendi, and A. Ali, “The use of a human body model to determine the variation of pathlosses in the human body channel in wireless capsule endoscopy,” *Prog. In Elec. Res.*, vol. 133, pp. 495–513, 2013.

[5] K. Takizawa, H. Hagiwara, and K. Hamaguchi, “Design of a radio system for capsule endoscopy through a pathloss analysis,” in *6th European Conf. Ant. and Propag. (EUCAP 2012)*, Mar. 2012, pp. 553–556.

[6] “Draft standard for local and metropolotan area networks part 15.6: Wireless body area networks,” *IEEE P802.15.6/ D05*, Oct. 2011.

[7] D. Nikolayev, M. Zhadobov, L. L. Coq, P. Karban, and R. Sauleau, “Robust ultraminiature capsule antenna for ingestible and implantable applications,” *IEEE Tran. Ant. and Propag.*, vol. 65, no. 11, pp. 6107–6119, Nov. 2017.

[8] Z. Bao, Y. Guo, and R. Mittra, “Single-layer dual-/tri-band inverted-F antennas for conformal capsule type of applications,” *IEEE Tran. Ant. and Propag.*, vol. 65, no. 12, pp. 7257–7265, Dec 2017.

[9] Y. Mahe, A. Chousseaud, M. Brunet, and B. Froppier, “New flexible medical compact antenna: Design and analysis,” *Int. J. Ant. and Propag.*, vol. 2012, no. 837230, p. 6 pages, 2012.

[10] R. Chávez-Santiago, C. Garcia-Pardo, A. Fornes-Leal, A. Vallés-Lluch, G. Vermeeren, W. Joseph, I. Balasingham, and N. Cardona, “Experimental path loss models for in-body communications within 2.36-2.5 GHz,” *IEEE J. Bio. and Health Infor.*, vol. 19, no. 3, pp. 930–937, May 2015.

[11] K. Lopez-Linares Roman, G. Vermeeren, A. Thielens, W. Joseph, and L. Martens, “Characterization of path loss and absorption for a wireless radio frequency link between an in-body endoscopy capsule and a receiver outside the body,” *EURASIP J. Wireless Commun. and Net.*, vol. 2014, no. 1, p. 21, 2014.

[12] C. Liu, Y. X. Guo, and S. Xiao, “Circularly polarized helical antenna for ISM-band ingestible capsule endoscope systems,” *IEEE Trans. Ant. and Propag.*, vol. 62, no. 12, pp. 6027–6039, Dec. 2014.

[13] K. M. S. Thotahewa, J. M. Redoutè, and M. R. Yuce, “Propagation, power absorption, and temperature analysis of UWB wireless capsule endoscopy devices operating in the human body,” *IEEE Trans. Micro. Theo. Tech.*, vol. 63, no. 11, pp. 3823–3833, Nov. 2015.

[14] Y. Morimoto, D. Anzai, and J. Wang, “Design of ultra wide-band low-band implant antennas for capsule endoscope application,” in *7th Int. Sym. Med. Infor. and Comm. Tech. (ISMICT)*, Mar. 2013, pp. 61–65.

[15] P. A. Floor, R. Chávez-Santiago, S. Brovoll, O. Aardal, J. Bergsland, O. J. H. N. Grymyr, P. S. Halvorsen, R. Palomar, D. Plettemeier, S. E. Hamran, T. A. Ramstad, and I. Balasingham, “In-body to on-body ultrawideband propagation model derived from measurements in living animals,” *IEEE J. Bio. and Heal. Infor.*, vol. 19, no. 3, pp. 938–948, May 2015.

[16] A. Alomainy and Y. Hao, “Modeling and characterization of biotelemetric radio channel from ingested implants considering organ contents,” *IEEE Trans. Ant. and Propag.*, vol. 57, no. 4, pp. 999–1005, Apr. 2009.

[17] M. S. Arefin, J. M. Redoute, and M. R. Yuce, “Meandered conformal antenna for ISM-band ingestible capsule communication systems,” in *38th Annual Int. Conf. of the IEEE Eng. in Med. and Bio. Soc. (EMBC)*, Aug. 2016, pp. 3031–3034.

[18] Z. Bao, Y. Guo, and R. Mittra, “An ultrawideband conformal capsule antenna with stable impedance matching,” *IEEE Trans. Ant. and Propag.*, vol. 65, no. 10, pp. 5086–5094, Oct. 2017.

[19] A. Khaleghi and I. Balasingham, “Improving in-body ultra wideband communication using near-field coupling of the implanted antenna,” *Microw. Opt. Technol. Lett.*, vol. 51, pp. 585–589, Jan. 2009.

[20] L. Xu, M. Q. H. Meng, H. Ren, and Y. Chan, “Radiation characteristics of ingestible wireless devices in human intestine following radio frequency exposure at 430, 800, 1200, and 2400 MHz,” *IEEE Trans. Ant. and Propag.*, vol. 57, no. 8, pp. 2418–2428, Aug. 2009.

[21] L. Xu, M. Q. H. Meng, and Y. Chan, “Effects of dielectric parameters of human body on radiation characteristics of ingestible wireless device at operating frequency of 430 MHz,” *IEEE Trans. Biomed. Engineering*, vol. 56, no. 8, pp. 2083–2094, Aug. 2009.

[22] L. C. Chirwa, P. A. Hammond, S. Roy, and D. R. S. Cumming, “Radiation from ingested wireless devices in biomedical telemetry bands,” *Elect. Let.*, vol. 39, no. 2, pp. 178–179, Jan. 2003.

[23] A. Khaleghi and I. Balasingham, “Wireless communication link for capsule endoscope at 600 MHz,” in *37th Annual Int. Conf. of the IEEE Eng. in Med. and Bio. Soc. (EMBC)*, Aug. 2015, pp. 4081–4084.

[24] F. E. Hatmi, M. Grzeskowiak, T. Alves, S. Protat, and O. Picon, “Magnetic loop antenna for wireless capsule endoscopy inside the human body operating at 315 MHz: Near field behavior,” in *11th Mediterranean Micro. Symp. (MMS)*, Sept. 2011, pp. 81–87.

[25] F. Merli, L. Bolomey, J. F. Zurcher, G. Corradini, E. Meurville, and A. K. Skrivervik, “Design, realization and measurements of a miniature antenna for implantable wireless communication systems,” *IEEE Trans. Ant. and Propag.*, vol. 59, no. 10, pp. 3544–3555, Oct. 2011.

[26] B. Huang, G. Z. Yan, and P. Zan, “Design of ingested small microstrip antenna for radiotelemetry capsules,” *Elec. Let.*, vol. 43, no. 22, Oct. 2007.

[27] S. I. Kwak, K. Chang, and Y. J. Yoon, “The helical antenna for the capsule endoscope,” in *IEEE Ant. and Propag. Soc. Int. Sym.*, vol. 2B, July 2005, pp. 804–807.

[28] S. I. Kwak, K. Chang, and Y. j. Yoon, “Small spiral antenna for wideband capsule endoscope system,” *Elec. Let.*, vol. 42, no. 23, pp. 1328–1329, Nov. 2006.

[29] S. Lee and Y. Yoon, “Fat arm spiral antenna for wideband capsule endoscope systems,” in *IEEE Rad. Wire. Sym. (RWS)*, 10-14 Jan. 2010, pp. 579–582.

[30] S. H. Lee, K. Chang, and Y. J. Yoon, “A dual spiral antenna for wideband capsule endoscope system,” in *Asia-Pacific Microwave Conf.*, Dec. 2007, pp. 1–4.

[31] S. H. Lee, K. Chang, K. J. Kim, and Y. J. Yoon, “A conical spiral antenna for wideband capsule endoscope system,” in *IEEE Ant. and Propag. Soc. Int. Sym.*, July 2008, pp. 1–4.

[32] S. H. Lee, J. Lee, Y. J. Yoon, S. Park, C. Cheon, K. Kim, and S. Nam, “A wideband spiral antenna for ingestible capsule endoscope systems: Experimental results in a human phantom and a pig,” *IEEE Trans. Biomed. Engineering*, vol. 58, no. 6, pp. 1734–1741, June 2011.

[33] S. H. Lee and Y. J. Yoon, “A dual spiral antenna for ultra-wideband capsule endoscope system,” in *Int. Workshop Ant. Tech.: Small Antennas and Novel Metamaterials*, Mar. 2008, pp. 227–230.

[34] J. Faerber, G. Cummins, S. K. Pavuluri, P. Record, A. R. A. Rodriguez, H. S. Lay, R. McPhillips, B. F. Cox, C. Connor, R. Gregson, R. E. Clutton, S. R. Khan, S. Cochran, and M. P. Y. Desmulliez, “In vivo characterization of a wireless telemetry module for a capsule endoscopy system utilizing a conformal antenna,” *IEEE Trans. Bio. Cir. and Sys.*, vol. PP, no. 99, pp. 1–11, 2017.

[35] A. Konstantinos, A. Kiourti, and K. Nikita, “A novel conformal antenna for ingestible capsule endoscopy in the MedRadio band,” in *Prog. in Elec. Res. Sym. Proc.*, Stockholm, Sweden, Aug. 2013.

[36] X. Cheng, J. Wu, R. Blank, D. E. Senior, and Y. K. Yoon, “An omnidirectional wrappable compact patch antenna for wireless endoscope applications,” *IEEE Ant. and Wireless Propag. Lett.*, vol. 11, pp. 1667–1670, 2012.

[37] L. J. Xu, Y. X. Guo, and W. Wu, “Bandwidth enhancement of an implantable antenna,” *IEEE Ant. and Wireless Propag. Lett.*, vol. 14, pp. 1510–1513, 2015.

[38] R. Das and H. Yoo, “A wideband circularly polarized conformal endoscopic antenna system for high-speed data transfer,” *IEEE Tran. Ant. and Propag.*, vol. 65, no. 6, pp. 2816–2826, June 2017.

[39] Y. Sumin, K. Kihyun, and N. Sangwook, “Outer-wall loop antenna for ultrawideband capsule endoscope system,” *IEEE Ant. Wireless Propag. Lett.*, vol. 9, pp. 1135–1138, 2010.

[40] J. Wang, M. Leach, E. G. Lim, Z. Wang, R. Pei, and Y. Huang, “An implantable and conformal antenna for wireless capsule endoscopy,”

IEEE Ant. and Wireless Propag. Lett., vol. 17, no. 7, pp. 1153–1157, July 2018.

[41] R. Alrawashdeh, Y. Huang, and G. Ping C.and Eng, "A new small conformal antenna for capsule endoscopy," in *7th European Conf. Ant. Propag. (EuCAP 2013)*, Gothenburg, Sweden, Apr. 2013, pp. 220–223.

[42] R. S. Alrawashdeh, Y. Huang, M. Kod, and A. A. B. Sajak, "A broadband flexible implantable loop antenna with complementary split ring resonators," *IEEE Ant. and Wireless Propag. Lett.*, vol. 14, pp. 1506–1509, 2015.

[43] X. Cheng, D. E. Senior, C. Kim, and Y. K. Yoon, "A compact omnidirectional self-packaged patch antenna with complementary split-ring resonator loading for wireless endoscope applications," *IEEE Ant. and Wireless Propag. Lett.*, vol. 10, pp. 1532–1535, 2011.

[44] P. Izdebski, H. Rajagopalan, and Y. Rahmat-Samii, "Conformal ingestible capsule antenna: A novel chandelier meandered design," *IEEE Trans. Ant. Propag.*, vol. 57, no. 4, pp. 900–909, Apr. 2009.

[45] J. C. Wang, E. G. Lim, Z. Wang, Y. Huang, T. Tillo, M. Zhang, and R. Alrawashdeh, "UWB planar antennas for wireless capsule endoscopy," in *Int. Workshop Ant. Tech. (iWAT)*, Mar. 2013, pp. 340–343.

[46] C. Roopnariane, M. Tofighi, and C. Collins, "Radiation performance of small implanted antennas in head at MICS, ISM, and GPS bands," in *Proc. IEEE 36th Annual Northeast Bio. Conf.*, 2010, pp. 1–2.

[47] S. Park, W. Kim, J. Lee, Y. seek Chung, and C. Cheon, "A new receiver antenna with buffer layer for wireless capsule endoscopy in human body," in *IEEE Ant. and Propag. Soc. Int. Sym.*, Jul. 2008, pp. 1–4.

[48] A. Kiourti, J. R. Costa, C. A. Fernandes, and K. S. Nikita, "A broadband implantable and a dual-band on-body repeater antenna: Design and transmission performance," *IEEE Trans. Ant. and Propag.*, vol. 62, no. 6, pp. 2899–2908, June 2014.

[49] K. Kwon, J. Ha, S. Lee, and J. Choi, "Design of a dual-band on-body antenna for a wireless body area network repeater system," *Int. J. Ant. and Propag.*, vol. 2012, pp. 418–421, 2012.

[50] S. Yan, V. Volskiy, and G. A. E. Vandenbosch, "Compact dual-band textile pifa for 433-MHz/2.4-GHz ISM bands," *IEEE Ant. and Wireless Propag. Lett.*, vol. 16, pp. 2436–2439, 2017.

[51] L. J. Xu, Z. Duan, Y. M. Tang, and M. Zhang, "A dual-band on-body repeater antenna for body sensor network," *IEEE Ant. and Wireless Propag. Lett.*, vol. 15, pp. 1649–1652, 2016.

[52] M. S. Miah, K. Haneda, C. Icheln, A. Khatun, and K. I. Takizawa, "An ultrawideband conformal loop antenna for ingestible capsule endoscope system," in *10th European Conf. Ant. and Propag. (EuCAP 2016)*, Apr. 2016, pp. 1–5.

[53] F. Merli, "Implantable antennas for biomedical applications," Ph.D. dissertation, Ecole Polytechnique Fédérale de Lausanne (EPFL), Switzerland, Sep. 2011. [Online]. Available: http://infoscience.epfl.ch/record/166129/files/EPFL_TH5110.pdf

[54] C. Gabriel, *Compilation of the dielectric properties of body tissues at RF and microwave frequencies*. Brooks Air Force Base, Texas (USA), Tech. Rep. Report N.AL/OE-TR-, June 1996.

[55] H. Rajagopalan and Y. Rahmat-Samii, "Wireless medical telemetry characterization for ingestible capsule antenna designs," *IEEE Ant. and Wireless Propag. Lett.*, vol. 11, pp. 1679–1682, 2012.

[56] "IEEE standard for safety levels with respect to human exposure to radio frequency electromagnetic fields, 3 KHz to 300 GHz," *IEEE Standard C95.1-1999*, 1999.

[57] "IEEE standard for safety levels with respect to human exposure to radio frequency electromagnetic fields, 3 KHz to 300 GHz," *IEEE Standard C95.1-2005*, 2005.

[58] "Short range devices (SRD) operating in the frequency range 25 MHz to 1000 MHz," *document ETSI EN 300 220*, Nov. 2016.

[59] M. Nesasudha and D. Mathew, "Effect of partial ground plane on the microstrip patch antenna performance for wireless sensor networks," *J. Elec. Design. Tech.*, vol. 4, no. 3, 2013.

[60] P. C. Ooi and K. T. Selvan, "The effect of ground plane on the performance of a square-loop CPW-fed printed antenna," *Prog. In Electromag. Res. Lett.*, vol. 19, 2010.

[61] D. Priyanka and S. A. Shirsat, "Bandwidth enhancement of microstrip antenna using partial ground," *Int. J. Sci. and Eng. Res.*, vol. 4, no. 11, Nov. 2013.

[62] R. Anane, K. Raoof, and R. Bouallegue, "On the evaluation of GMSK scheme with ECC techniques in wireless sensor network," *Int. J. Wireless and Mob. Net.*, vol. 7, no. 2, 2015.

Md. Suzan Miah was born in Gazipur, Bangladesh, in 1985. He received the B.Sc. (Tech.) (with Summa Cum Laude distinction) in Electrical and Electronics Engineering from American International University Bangladesh in 2008 and M.Sc. (Tech.) (with distinction) degree in Radio Science and Engineering from School of Electrical Engineering, Aalto University, Finland in 2014. He is currently working toward the D.Sc. (Tech.) degree at Aalto University. Since 2013, he has been with the Department of Electronics and Nanoengineering, School of Electrical Engineering, Aalto University, initially as a Research Assistant and now as a Doctoral candidate.

His research interests include antenna systems for medical applications, millimeter-wave antenna solutions, and over-the-air antenna testing.

Ahsan Noor Khan was born in Faisalabad, Pakistan, in 1987. He received the B.Sc. degree in communication systems from Institute of Space Technology Islamabad, Pakistan, in 2009, the M.Sc. degree (with distinction) in radio science and engineering from Aalto University, Espoo, Finland, in 2016. He is currently pursuing his Ph.D. degree with the Department of Electronics Engineering and Computer Science, Queen Mary University of London, United Kingdom. His current research interests include implantable and wearable antenna systems, and RF triggered medical devices.

Clemens Icheln received the M.Sc. degree in Electrical Engineering (Dipl.-Ing.) at Hamburg-Harburg University of Technology, Germany, in 1996, the Licentiate degree in Radio Engineering and the Doctor of Science in Technology degree at Helsinki University of Technology (now: Aalto University), Finland, in 1999 and 2001, respectively. He is currently working as University Lecturer at the Department of Electronics and Nanoengineering of Aalto University School of Electrical Engineering. His main research interests are the design of multi-element antennas for small communications devices such as mobile terminals and medical implants, to operate at frequency ranges as low as 400 MHz but also up to mm-wave frequencies, as well as the development of suitable antenna characterisation methods that allow taking e.g. the radio channel into account.

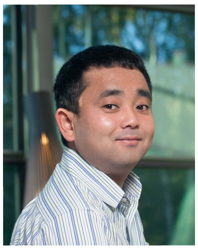

Katsuyuki Haneda (S'03, M'07) received the Doctor of Engineering from the Tokyo Institute of Technology, Tokyo, Japan, in 2007. Dr. Haneda is presently an associate professor in Aalto University School of Electrical Engineering. He is the author and co-author of a number of best paper awards in IEEE Vehicular Technology Conference, European Conference on Antennas and Propagation and Loughborough Antennas and Propagation Conference, including student paper awards. Dr. Haneda has been an associate editor of the IEEE Transactions on Antennas and Propagation between 2012 and 2016, and of an editor of the IEEE Transactions on Wireless Communications since 2013. He has also been an active member of a number of European COST Actions, e.g., CA15104 "Inclusive Radio Communication Networks for 5G and beyond (IRACON)", where he is a co-chair of a disciplinary working group on radio channels. His current research activity includes high-frequency radios such as millimeter-wave and beyond, wireless for medical, post-disaster scenarios and internet-of-things, and in-band full-duplex radio technologies.

K. Takizawa received the B.E., M.E., and Ph.D. degrees in engineering from Niigata University, Niigata, Japan, in 1998, 2000, and 2003, respectively. He joined the National Institute of Information and Communications Technology (NICT) in 2003. Since 2016, he has been a Research Manager at NICT.